Applied Acoustics 177 (2021) 107928

Contents lists available at ScienceDirect

Applied Acoustics

journal homepage: www.elsevier.com/locate/apacoust

In-situ prediction of α-phase volume fraction in titanium alloy using laser ultrasonic with support vector regression

Dan Chen [a,b,c], Yanjun Liu [e], Wei Feng [b,d,*], Yuanhao Wang [f], Qing Hu [f], Gaolong Lv [a,b,c], Shuxiao Zhang [a,b,c], Shifeng Guo [a,b,c,d,*]

[a] Shenzhen Key Laboratory of Smart Sensing and Intelligent Systems, Shenzhen Institutes of Advanced Technology, Chinese Academy of Sciences, Shenzhen 518055, China
[b] Guangdong Provincial Key Lab of Robotics and Intelligent System, Shenzhen Institutes of Advanced Technology, Chinese Academy of Sciences, Shenzhen 518055, China
[c] CAS Key Laboratory of Human-Machine Intelligence-Synergy Systems, Shenzhen Institutes of Advanced Technology, Shenzhen 518055, China
[d] University of Chinese Academy of Sciences, Beijing 100049, China
[e] Department of Electrical and Electronic Engineering, Southern University of Science and Technology, Shenzhen 518055, China
[f] SUSTech Engineering Innovation Center, School of Environmental Science and Engineering, Southern University of Science and Technology, Shenzhen 518055, China

ARTICLE INFO

Article history:
Received 4 December 2020
Received in revised form 22 December 2020
Accepted 11 January 2021

Keywords:
Laser ultrasonics
Rayleigh ultrasonic wave
Support vector regression
α-Phase fraction
Titanium alloys
Phase transformations

ABSTRACT

A laser ultrasonic based non-contact detection method combined with support vector regression (SVR) was proposed for the first time for in-situ predicting the volume fraction of α-phase in titanium alloy (Ti-10V-2Fe-3Al). The alloy specimens were heated with incremental temperatures from 820 to 1100 °C to obtain different microstructures and volume fraction of α-phase, and the nonlinear relationship between the parameter of Rayleigh ultrasonic wave (velocity, amplitude and peak frequency) and the volume fraction of α-phase was established and analyzed by the combination of laser ultrasonic experiment and metallographic analysis. The SVR, with ultrasonic parameters and heat treatment parameters (heating and cooling rate, holding time and holding temperature) as input features, was implemented to predict the volume fraction of α-phase, achieving a relative mean error less than 5%. The results indicate that the SVR-based laser ultrasonic technique can be applied as a reliable and effective method for in-situ characterization of volume fraction of α-phase in titanium alloy.

1. Introduction

Titanium alloy has excellent comprehensive properties, such as high specific strength and fracture toughness, fatigue strength and resistance to crack propagation, which has been widely used in aviation, aerospace and other industrial departments [1–4]. According to the micro-structures, titanium alloys can be divided into α, β and α + β titanium alloys. The micro-structural features, such as grain size, texture, phase constitution that are closely related to mechanical performance of titanium alloys, are significantly affected by heat treatment conditions [5,6]. Rapid characterization and even real-time monitoring of phase transition and microstructure evolution could be helpful for improving production process and optimizing material properties. The conventional approach for characterizing the micro-structures involves a battery of cumbersome and time-consuming processes that using either scanning electron microscopy (SEM), electron backscatter diffraction (EBSD), X-ray diffraction, mechanical testing or their combination, which are off-line based, and some dynamic processes, such as recrystallization, phase transition and subsequent grain growth that are of great significance for the optimization of production process cannot be discerned in time [7–10].

The non-contact laser ultrasonic (LU) technology, using a pulsed laser to generate ultrasonic waves and utilizing an optical interferometer to detect ultrasonic waves has been widely implemented for evaluating microstructures, such as texture coefficient [11,12], grain size [6,13,14], porosity [15,16], and crystal elasticity constants [17–19]. The LU technique is insensitive to environment factors, such as high temperature, heavy electromagnetic interference, and vibration, etc. [20–23]. Due to these merits, the LU technique has created various opportunities for the application of data-driven methods for phase transformation monitoring [24,25], mechanical performance evaluation [17] and microstructure characterization [26]. Most recently, the in-process monitoring of additive manufacturing using the generated high frequency ultrasonic waves to characterize micro-defects and residual stress have been published elsewhere [27–29].

* Corresponding authors at: Guangdong Provincial Key Lab of Robotics and Intelligent System, Shenzhen Institutes of Advanced Technology, Chinese Academy of Sciences, Shenzhen 518055, China.
E-mail addresses: wei.feng@siat.ac.cn (W. Feng), sf.guo@siat.ac.cn (S. Guo).

https://doi.org/10.1016/j.apacoust.2021.107928
0003-682X/

The parameters of laser-generated ultrasonic waves, such as velocity, attenuation and frequency that closely correlate with the microstructures, have been widely used for materials characterization [30,31]. Maalekian et al. [13] proposed a novel in situ ultrasonic technique to measure the austenite grain grown during continuous heating and subsequent isothermal holding at various temperatures in the range of 950–1250 °C. Dong et al. [6] reported a novel model to calculate the log-normal distribution of grain size based on the correlation between the frequency dependent attenuation and the volumetric grain size distribution of Ti alloy. Scattering and attenuation of longitudinal and transverse waves with microstructure or microtextural of single phase and duplex polycrystalline materials have been studied [32,33]. Based on velocity dispersion, the grain growth, texture type and feature measurement of anisotropic materials using LU have also been investigated [11,13,15]. However, above methods mainly rely on the correlation between one or several parameters of ultrasonic waves and the microstructure of single phase polycrystalline materials. For multiphase materials with different microstructures, the variation of wave velocity and amplitude resulting from the multi-factor coupling related to the microstructures and phases is more complicated, which making it difficult and inaccurate to evaluate the microstructure of material from the direct ultrasound data.

The development of machine learning (ML) and artificial intelligence (AI) technology has provided new possibilities for accelerating materials design and characterization [34–36]. It avoids building complex model by using costly, time-consuming experimental trials or physical theoretical calculations, but with the help of high-performance computing and high-dimension, large-size industrial datasets for well mapping the complex nonlinear relationship between the micro-structure information and parameters of ultrasonic signals. The ML and multi-scale calculation has been combined for predicting the tensile strength of pearlitic steel wires using industrial data [35]. Time-frequency patterns of acoustic emission (AE) signals have been put into ML models to predict the salient microstructural phases present on a metallic workpiece surface [37]. However, the usage of ML to assist in characterizing the microstructure of multiphase alloy materials by laser ultrasound has not been reported.

In this work, an in situ microstructure characterization method that combines LU technique and machine learning method is proposed for predicting the α-phase fraction of titanium alloy, Ti-10V-2Fe-3Al. The alloy specimens are heated with incremental temperatures to obtain different duplex microstructures of α-phase and β-phase. The relationship between the fraction of α-phase and the parameters of Rayleigh ultrasonic waves is established by the combination of laser ultrasonic experiment and metallographic analysis, and the support vector regression (SVR) algorithm is further proposed for predicting the α-phase fraction. The rest of the paper is organized as follows. Section 2 describes the process of sample preparation and methods, including heat treatment of materials, laser ultrasonic experiment and support vector regression algorithm. Section 3 presents the results and discussion of LU experiments, materials characterization and prediction performance using SVR model. The conclusions of this work is summarized in Section 4.

2. Sample preparation and methods

2.1. Heat treatment of materials

The Ti-10V-2Fe-3Al alloy is a typical metastable β-type titanium alloy, which has high-strength/toughness and deep hardness. The volume fraction of α-phase is a critical parameter that influences the growth of β grain and the critical stress levels for the stress-induced martensitic transformation [5,38]. For obtaining different volume fraction of α-phase, six forged Ti-10V-2Fe-3Al specimens measuring 60 mm in length, 50 mm in width and 10 mm in thickness were undergone continuous heating in a muffle furnace (KSL-1750X-S, HF-Kejing, China), held at different temperature above β-transus temperature (metallographically measured at 793 °C), and followed by furnace cooling. The specific heating regime is shown in Table 1. Before laser ultrasonic experiment, the surface oxidation layer of each specimen is removed and the roughness of the specimen surface was kept consistent about 1 μm. After ultrasonic data acquisition, the specimen surface was polished and etched in a mixed solution of 10% hydrofluoric acid, 30% nitric acid for 5 s for metallographic observation. The vibration polishing was conducted to eliminate the residual stress, and avoid phase transition and preferred orientation. The phase constitutions of each specimen were examined using X-ray diffraction (XRD, Bruker D8 Discover) with Cu Kα radiation and the morphology of the duplex microstructure was analyzed using field emission scanning electron microscope (FESEM, ZEISS SUPRA®55).

2.2. Laser ultrasonic experiment

The schematic of laser ultrasonic setup is shown in Fig. 1. A Nd:YAG laser (Centurion+, Quantel Laser company, USA) with pulse duration of 12 ns, wavelength of 1064 nm is used to generate Rayleigh waves. To avoid ablation of material surface while enhancing signal intensity, the pulse energy is limited to 5 mJ and focused as a line with length about 10 mm. A double-wave mixed (DWM) interferometer (TEMPO 2D, Sound & Bright company, USA) with a continuous laser operating at wavelength of 532 nm and a bandwidth of 20 MHz is applied to receive the surface displacements. A bandpass filter of 532 nm is attached to the front of the interferometer lens to avoid the generation of disturbance signal by the pulsed laser. The DWM interferometer is synchronized with the Nd:YAG pulsed laser for signal acquisition. The distance between the generation and detection point is set at 22 mm, and the acoustic interrogation area is larger than 220 mm^2, which guarantee the reliability of the evaluation results. The data acquisition card (DAQ) has sampling frequency of 250 MHz and the received signal is averaged 128 times to improve the signal-to-noise ratio. The two-dimensional motion platform is used to move the sample to realize the scanning detection at different positions.

2.3. Support vector regression algorithm

The support vector regression (SVR) is based on the structural risk minimization (SRM) principle, which has greater generalization ability and is superior to the empirical risk minimization (ERM) principle as adopted in neural networks [38]. The SVR algorithm has been proven to be an effective tool in real-value function estimation. As a supervised-learning approach, SVR uses a symmetrical loss function, which equally penalizes high and low misestimates. One of the main advantages of SVR is that its computational complexity does not depend on the dimensionality of the input space. Additionally, it has excellent generalization capability and high prediction accuracy. Due to the complexity between acoustic parameters and volume fraction of α-phase, the SVR method is used to predict the volume fraction of α-phase. The flow chart for the prediction of the volume fraction of α-phase using SVR-based LU method is shown in Fig. 2. The acoustic parameters of Rayleigh ultrasonic waves: velocity, amplitude and peak frequency, and the heat treatment parameters: heating and cooling rate, holding time and holding temperature are extracted together as feature parameters, which are combined with the known label of α-phase fraction for training the SVR model. A total number of 66 signals were collected at different positions from the center of

Table 1
The heating regime of the Ti-10V-2Fe-3Al titanium alloy specimens.

No.	0	1	2	3	4	5
Holding temperature (°C)	RT	820	820	900	1000	1100
Heating rate (°C/min)	–	10	10	10	10	10
Holding time (min)	–	30	60	60	60	60

*RT represents room temperature.

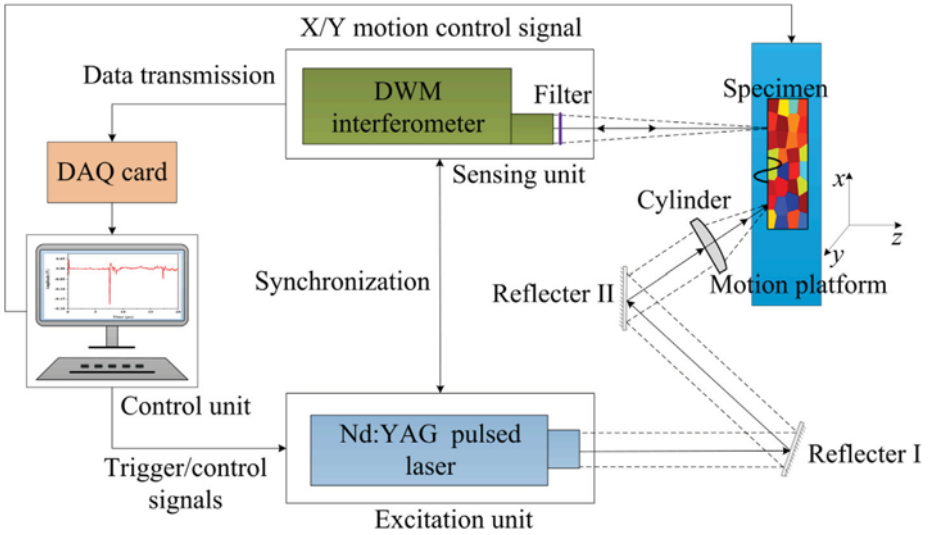

Fig. 1. The schematic diagram of laser ultrasonic technique for Rayleigh ultrasonic waves generation and detection on Ti-alloy specimens.

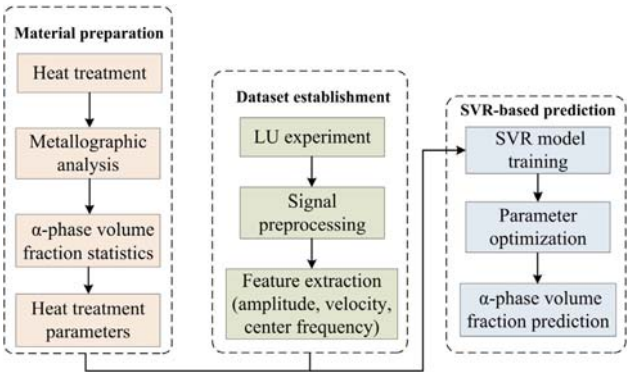

Fig. 2. Flow chart for predicting the α-phase fraction of Ti alloys using SVR-based laser ultrasonic method.

each specimen randomly, with 55 of them randomly selected as training set, and the remaining 11 used as testing set.

The idea of regression problem is to determine a function that can predict future values accurately. The generic SVR estimating function takes the form [39]

$$f(x) = (w \cdot \Phi(x)) + b \tag{1}$$

where, $w \subseteq R^n$, $b \subseteq R$, and Φ denotes a nonlinear transformation from R^n to high dimensional features space. The key point is to find the value of w and b such that values of x can be determined by minimizing the regression risk

$$R_{reg}(f) = C\sum_{i=0}^{\ell}\Gamma(f(x_i) - y_i) + \frac{1}{2}\| w \|^2 \tag{2}$$

where $\Gamma(\cdot)$ is a cost function, C a cost parameter. The vector w in Eq. (2) can be written in terms of data points as

$$w = \sum_{i=0}^{\ell}(\alpha_i - \alpha_i^*)\Phi(x_i) \tag{3}$$

And the generic Eq. (1) can be rewritten as

$$\begin{aligned} f(x) &= \sum_{i=1}^{\ell}(\alpha_i - \alpha_i^*)(\Phi(x_i)\cdot\Phi(x)) + b \\ &= \sum_{i=1}^{\ell}(\alpha_i - \alpha_i^*)k(x_i, x) + b \end{aligned} \tag{4}$$

In Eq. (4), the dot product can be replaced with function $k(x_i, x)$, so-called the kernel function. In this work, the radial basis function (RBF) is used as the kernel for regression

$$k(x_i, x) = \exp\left\{-\gamma|x - x_i|^2\right\} \tag{5}$$

where, γ is the kernel parameter.

3. Results and discussion

3.1. Microstructure characterization

Fig. 3(a)–(f) shows the morphology of microstructure of the Ti-alloy after heat treatment. All the six specimens consist of α + β phase, identified by the XRD pattern in Fig. 3(g). The dark and bright regions represent the α-phase and β-phase respectively. Due to forging work, the morphology of α-phase and β-phase in the as-received specimen 0# has elongated shape, as shown in Fig. 3(a). After recrystallization above β-phase transition temperature, the morphology of α-phase and β-phase was reshaped, with irregular colonies of β-phase near α-phase grain boundary, shown in Fig. 3(b) and (c). When the heating temperature exceeded

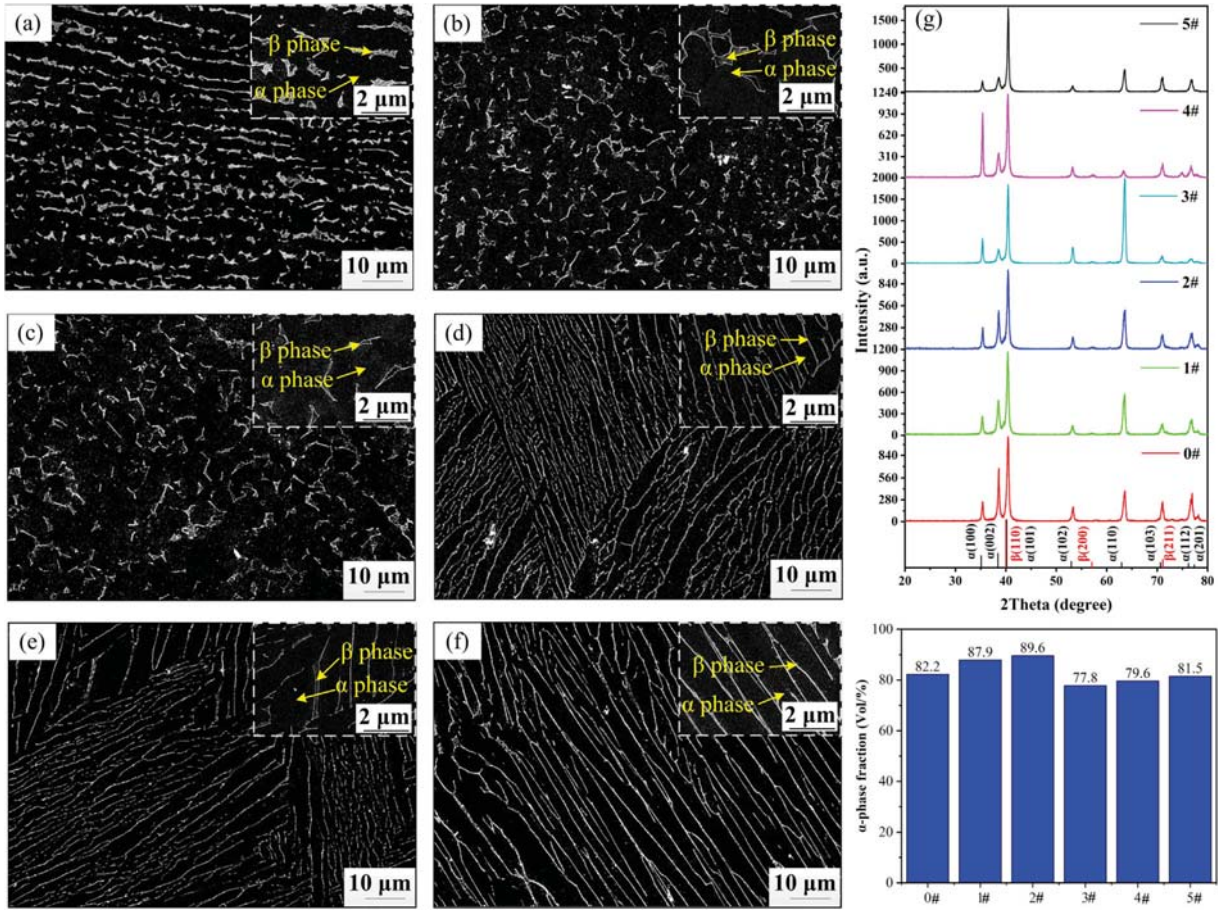

Fig. 3. Microstructural analysis: (a)-(f) show the SEM photographs of the representative microstructure for each specimen; (a) As-received specimen 0# at forged state; (b) specimen 1# at 820 °C for 0.5 h; (c) specimen 2# at 820 °C for 1.0 h; (d) specimen 3# at 900 °C for 1.0 h; (e) specimen 4# at 1000 °C for 1.0 h; (f) specimen 5# at 1100 °C for 1.0 h. The inset in each subplot shows the magnified microstructures and the α-phase and β-phase is marked with arrows; (g) the XRD patterns of 0#-5# specimens; (h) the volume fraction of α-phase in each specimen.

900 °C, the morphology of microstructure was changed significantly, with lath-shaped α-phase grain separated by the fine lamellar strips of β-phase, as shown in Fig. 3(d)–(f). The fraction of α-phase was quantitatively evaluated from the SEM micrographs using a binary imaging algorithm. Six different fields of view obtained from the center of the region of laser ultrasonic inspection with magnification of 100× are counted, with a total area of about 5.5 mm^2 in each specimen. It can be seen from Fig. 3(h) that the fraction of α-phase in specimens 0#–5# ranges from 77.8% to 89.6%.

3.2. Ultrasonic parametric analysis

Fig. 4(a) shows the representative waveform of the laser-generated Rayleigh ultrasonic waves, which is identified by the velocity according to the travel distance (22 mm) and arrival time. Fig. 4(b) is the zoomed signal of Rayleigh in Fig. 4(a), which means the velocity of Rayleigh wave in each specimen is different. Except for the specimen 0#, the other specimens have isotropic structures (Fig. 3(b)–(f)) and no texture exists, confirmed by the XRD pattern, shown in Fig. 3(g). The change of velocity of Rayleigh wave in Fig. 4 (b) is therefore mainly affected by the microstructural morphology in titanium alloy. Fig. 4(c) shows the variation of Rayleigh wave velocity with the volume fraction of α-phase in each specimen. It can be seem that the velocity of Rayleigh in each specimen is almost consistent, with very short bar of 95% confidence interval (CI) counted using the 66 signals at different position in each specimen. The velocity of the 66 signals in the same specimen is almost constant, but which are obviously different between different specimens, with a maximum difference larger than 150 m/s (except for 0# specimen). The abruptly increased velocity of Rayleigh wave (about 2983 m/s) in specimen 0# is mainly related to the intrinsic residual stress resulting from dislocation networks in the microstructure of the as-received forged specimen [40]. These networks can be reduced through annealing treatment, leading to the release of residual stress in specimens 1#–5#.

The variation of amplitude of Rayleigh wave with the volume fraction of α-phase is shown in Fig. 4(d). It can be seen that the relationship between the amplitude of Rayleigh wave and the fraction of α-phase is nonlinear for the volume fraction of α-phase varies from 77.8% to 89.6%. In addition, the amplitude of Rayleigh wave in specimens 0#–2# is significantly higher than that in specimens 3#–5#, which is probably related to the morphology of α-phase, in Fig. 3(a)–(f). Fig. 4(e) shows the frequency spectrum of Rayleigh waves from specimens 0#–5#. It can be seen that Rayleigh wave has a broad frequency band ranging from 1 to 5 MHz and the variation of bandwidth for each specimen is obvious. According to the frequency spectrum in Fig. 4(e), the wavelength of Rayleigh wave in Ti-alloy is about 1.0 to 1.5 mm, indicating that the scattering of Rayleigh waves mainly occurs in the Rayleigh scattering regime, and following the relationship [6]

$$\alpha(\lambda, D) = C_R D^3 \lambda^{-4} \tag{6}$$

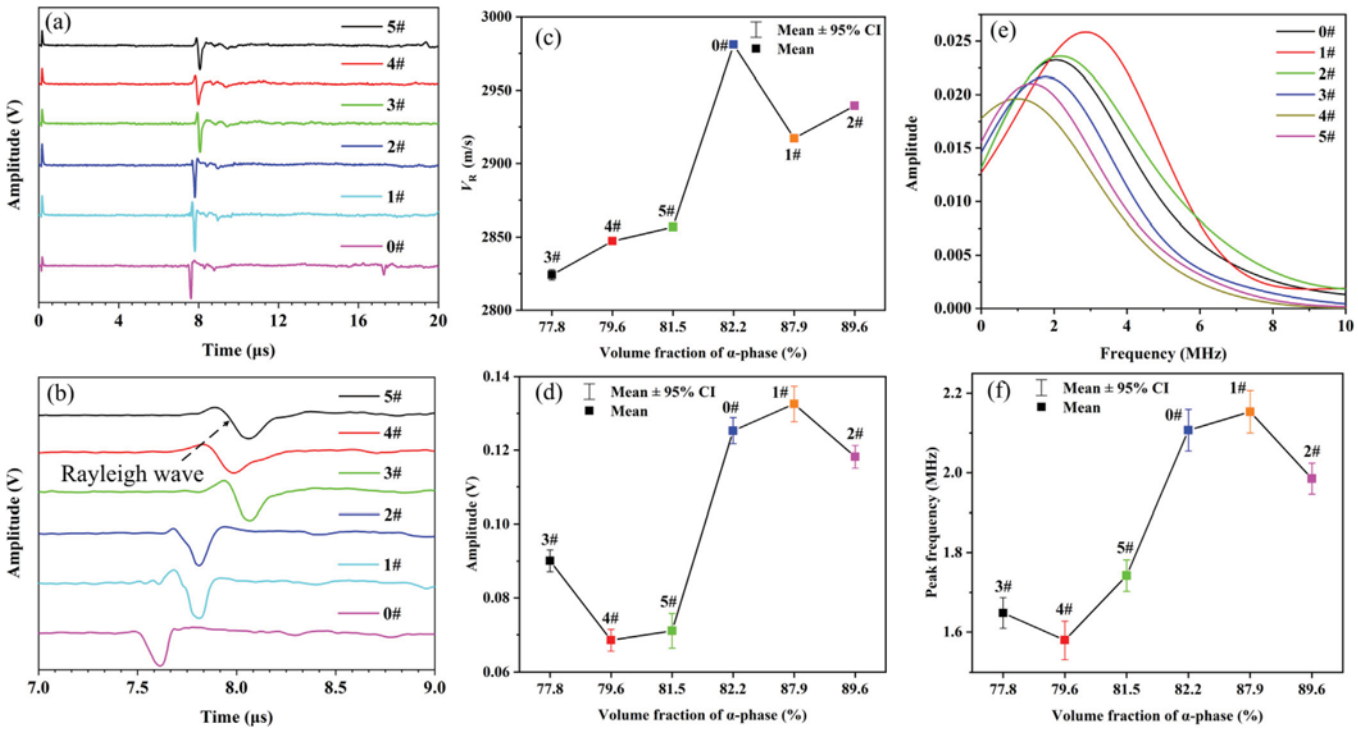

Fig. 4. Laser ultrasonic signal analysis: (a) the time-domain signals of the received ultrasonic waves from specimens 0#–5#; (b) the zoomed signal of Rayleigh wave in (a); (c), (d) the variation of velocity and amplitude of Rayleigh waves with volume fraction of α-phase; (e) the frequency spectrum of Rayleigh waves in each specimen; (f) the variation of peak frequency of Rayleigh waves with volume fraction of α-phase; the error bars show the 95% confidence interval for ultrasonic parameters at 66 different locations in each specimen.

where, α is the attenuation coefficient, C_R is material constant, D the mean grain size, λ the wavelength of ultrasound. Eq. (6) shows that the attenuation coefficient α is proportional to the minus fourth power of λ, when the α-phase in Ti-alloy has equiaxed crystal structures. Therefore, the preferential attenuation of higher frequencies causes the spectrum low-frequency offset, as shown in Fig. 4(e).

Take specimens 1# and 4# as an example, Fig. 4(e) shows that the high frequency components above 1.0 MHz in specimen 4# are reduced substantially when compared with specimen 1#. Combined with the duplex microstructure in specimens 1# and 4# [Fig. 3(b) and (d)], the low-frequency offset of spectrum indicates that the α-phase with lath shape is more likely to cause high-frequency attenuation than that with irregular colonies. For the Ti-alloy with duplex microstructure and approximate ellipsoidal grain, the explicit backscattering coefficient can be expressed as [26]:

$$\eta(\mathbf{k}) = \frac{(1 - M)Q_\beta V_\beta k^4}{\left(1 + 4k_x^2 a_\beta^2 + 4k_y^2 b_\beta^2 + 4k_z^2 c_\beta^2\right)^2} + MQ_\alpha V_\alpha k^4 \tag{7}$$

where, M represents a normalized average characteristic length, $Q_{\alpha,\beta}$ the normalized covariance of elastic stiffness, and $V_{\alpha,\beta}$ the "effective volumes" for α-phase and β-phase, k_i (i = x, y, z) the direction vector of incident wave, k the wavenumber. Eq. (7) indicates that the backscattering of ultrasonic waves from the α-phase with lath shape depends strongly on the incident wave direction. However, due to the random orientation of α-phase grain, the attenuation from a large detection area is proportional to the effective volume fractions of α-phase [41]. The relationship between peak frequency of Rayleigh wave and the volume fractions of α-phase is shown in Fig. 4(f). It can be seen that the relationship between the peak frequency of Rayleigh wave and the volume fractions of α-phase is nonlinear, which is similar as the feature parameter of amplitude in Fig. 4(d).

In summary, the three ultrasonic parameters present a complex relationship with the variation of volume fractions of α-phase, that leading to the directly evaluation of volume fractions of α-phase from ultrasonic signals is much difficult. In addition, the grain size and the morphology of α-phase and β-phase influence significantly on the three ultrasonic parameters due to the scattering and attenuation effects. Considering the correlation between the grain size, phase morphology and the heat treatment temperature, the heat treatment temperature was adopted as the important index for describing the grain size and phase morphology. And three parameters, including heating and cooling rate, holding time and holding temperature, combined with the three parameters of ultrasonic signals are selected as input features for predicting the volume fractions of α-phase using SVR model.

3.3. Prediction of volume fractions of α-phase using SVR

First, the cost parameter C and kernel function parameter γ in Eqs. (2) and (5) are determined using two-fold cross validation and further optimized with grid search method, with optimized value of 11.5 and 0.1, respectively. The index of relative mean error (RME) is applied for evaluating the performance of the SVR model [39]. Fig. 5 shows the RME of the volume fraction of α-phase predicted using the proposed SVR model. It can be seen that the RME of volume fraction prediction for specimens 0#–5# is less than 5%, which proves the effectiveness of the SVR-based laser ultrasonic method for evaluating the volume fraction of α-phase in titanium alloy.

4. Conclusions

In this work, an in-situ evaluation method for predicting the volume fractions of α-phase in Ti-10V-2Fe-3Al alloy is proposed, by the combination of laser ultrasonic technique and support vec-

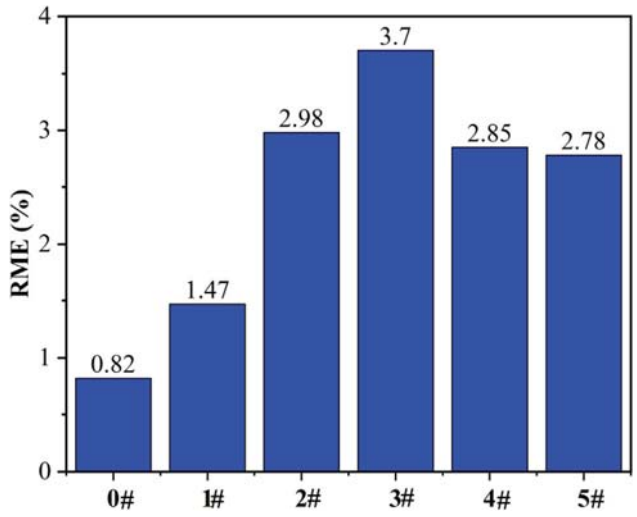

Fig. 5. RME of volume fraction of α-phase predicted using SVR-based laser ultrasonic method.

tor regression for the first time. The nonlinear relationship between the ultrasonic parameters (amplitude, velocity and peak frequency) of Rayleigh wave and the volume fraction of α-phase are obtained and analyzed. The SVR algorithm using the parameters of laser-generated Rayleigh ultrasonic wave and the heat treatment parameters as input features is proposed to predict the volume fraction of α-phase, which has a RME less than 5% for each specimen. This work proves that the SVR-based LU method can be considered as a powerful mean for in-situ evaluation of microstructure in multiphase metallic materials.

Declaration of Competing Interest

The authors declare that they have no known competing financial interests or personal relationships that could have appeared to influence the work reported in this paper.

Acknowledgements

This work was supported by the National Natural Science Foundation of China [grant number 52071332], Guangdong Frontier and Key Technological Innovation [grant number 2017B090910013], Science and Technology Innovation Commission of Shenzhen [grant numbers ZDSYS20190902093209795, JCYJ20170818153048647 and JCYJ 20180507182239617], the China Postdoctoral Science Foundation (grant number 2020M672891) and the Guangdong Basic and Applied Basic Research Foundation (grant number 2020A1515110218).

Author statement

Dan Chen implemented the experiments, analyzed the data and wrote the paper. Shifeng Guo and Wei Feng supervised the project, conceived the approach, and corrected the manuscript. Yanjun Liu guided the laser ultrasonic experiments, Yuanhao Wang and Qing Hu evaluated and commented on the results. Gaolong Lv and Shuxiao Zhang analyzed the data and provided valuable suggestions.

References

[1] Boyer RR, Briggs RD. The use of β Titanium alloys in the aerospace industry. J Mater Eng Perform 2005;14(6):681–5.
[2] Antunes RA, Salvador CAF, Oliveira MCL. Materials selection of optimized titanium alloys for aircraft applications. Mater Res 2018;21:1–9.
[3] Bobbili R, Madhu V. Effect of strain rate and stress triaxiality on tensile behavior of Titanium alloy Ti-10-2-3 at elevated temperatures. Mater Sci Eng A 2016;667:33–41.
[4] Cui C, Hu B, Zhao L, Liu S. Titanium alloy production technology, market prospects and industry development. Mater Des 2011;32(3):1684–91.
[5] Qi L, Qiao X, Huang L, Huang Xu, Zhao X. Effect of structural stability on the stress induced martensitic transformation in Ti-10V-2Fe-3Al alloy. Mater Sci Eng, A 2019;756:381–8.
[6] Dong F, Wang X, Yang Q, Liu H, Xu D, Sun Y, Zhang Y, Xue R, Krishnaswamy S. In-situ measurement of Ti-6Al-4V grain size distribution using laser-ultrasonic technique. Scr Mater 2018;154:40–4.
[7] Liang S, Levesque D, Legrand N, Zurob HS. Use of in-situ laser-ultrasonic measurements to develop robust models combining deformation, recovery, recrystallization and grain growth. Acta Mater 2020.
[8] Warchomicka F, Canelo-Yubero D, Zehetner E, Requena G, Stark A, Poletti C. In-situ synchrotron X-ray diffraction of Ti-6Al-4V during thermomechanical treatment in the beta field. Metals 2019;9:862.
[9] Bucsek AN, Casalena L, Pagan DC, Paul PP, Chumlyakov Y, Mills MJ, Stebner AP. Three-dimensional in situ characterization of phase transformation induced austenite grain refinement in nickel-titanium. Scr Mater 2019;162:361–6.
[10] Lhadi S, Purushottam raj purohit RRP, Richeton T, Gey N, Berbenni S, Perroud O, Germain L. Elasto-viscoplastic tensile behavior of as-forged Ti-1023 alloy: experiments and micromechanical modeling. Mater Sci Eng A 2020;787:139491.
[11] Zhang J, Yin A, Tao C, Wang Y, Zhu Z, Peng H, Shu X. Rapid measurement of the fourth-order texture coefficient by laser ultrasonic surface acoustic waves based on a neural network expert system. Appl Opt 2019;58:626.
[12] Bate P, Lundin P, Lindh-Ulmgren E, Hutchinson B. Application of laser-ultrasonics to texture measurements in metal processing. Acta Mater 2017;123:329–36.
[13] Maalekian M, Radis R, Militzer M, Moreau A, Poole WJ. In situ measurement and modelling of austenite grain growth in a Ti/Nb microalloyed steel. Acta Mater 2012;60:1015–26.
[14] Xue R, Wang X, Yang Q, Dong F, Zhang Y, Cao J, Song G. Grain size characterization of aluminum based on ensemble empirical mode decomposition using a laser ultrasonic technique. Appl Acoust 2019;156:378–86.
[15] Podymova NB, Kalashnikov IE, Bolotova LK, Kobeleva LI. Laser-ultrasonic nondestructive evaluation of porosity in particulate reinforced metal-matrix composites. Ultrasonics 2019;99:105959.
[16] Chen D, Lv G, Guo S, Zuo R, Liu Y, Zhang K, Su Z, Feng W. Subsurface defect detection using phase evolution of line laser-generated Rayleigh waves. Opt Laser Technol 2020;131:106410.
[17] Hutchinson B, Malmström M, Lönnqvist J, Bate P, Ehteshami H, Korzhavyi PA. Elasticity and wave velocity in fcc iron (austenite) at elevated temperatures – experimental verification of ab-initio calculations. Ultrasonics 2018;87:44–7.
[18] Toozandehjani M, Matori KA, Ostovan F, Mustapha F, Zahari NI, Oskoueian A. On the correlation between microstructural evolution and ultrasonic properties: a review. J Mater Sci 2015;50:2643–65.
[19] Zhan Yu, Liu C, Kong X, Li Y. Measurement of fiber reinforced composite engineering constants with laser ultrasonic. Appl Acoust 2018;139:182–8.
[20] Zhang K, Zhou Z. Quantitative characterization of disbonds in multilayered bonded composites using laser ultrasonic guided waves. NDT and E Int 2018;97:42–50.
[21] Tian J, Dong X, Gao S, Yao Y. Multipoint fiber-optic laser-ultrasonic actuator based on fiber core-opened tapers. Opt. Express 2017;25:29737.
[22] Zhan Yu, Li Y, Zhang E, Ge Y, Liu C. Laser ultrasonic technology for residual stress measurement of 7075 aluminum alloy friction stir welding. Appl Acoust 2019;145:52–9.
[23] Yi D, Pei C, Liu T, Chen Z. Inspection of cracks with focused angle beam laser ultrasonic wave. Appl Acoust 2019;145:1–6.
[24] Dubois M, Moreau A, Militzer M, Bussière JF. Laser-ultrasonic monitoring of phase transformations in steels. Scr Mater 1998;39:735–41.
[25] Dubois M, Moreau A, Bussière JF. Ultrasonic velocity measurements during phase transformations in steels using laser ultrasonics. J Appl Phys 2001;89:6487–95.
[26] Lobkis OI, Rokhlin SI. Characterization of polycrystals with elongated duplex microstructure by inversion of ultrasonic backscattering data. Appl Phys Lett 2010;96:161905.
[27] Zhan Yu, Liu C, Zhang J, Mo G, Liu C. Measurement of residual stress in laser additive manufacturing TC4 titanium alloy with the laser ultrasonic technique. Mater Sci Eng A 2019;762:138093.
[28] Cerniglia D, Scafidi M, Pantano A, Rudlin J. Inspection of additive-manufactured layered components. Ultrasonics 2015;62:292–8.
[29] Everton SK, Hirsch M, Stravroulakis P, Leach RK, Clare AT. Review of in-situ process monitoring and in-situ metrology for metal additive manufacturing. Mater Des 2016;95:431–45.
[30] Yin A, Yang Q, He F, Xiao H. Determination of grain size in deep drawing steel sheet by laser ultrasonics. Mater Trans 2014;55:994–7.
[31] Dong F, Wang X, Yang Q, Yin A, Xu X. Directional dependence of aluminum grain size measurement by laser-ultrasonic technique. Mater Charact 2017;129:114–20.
[32] Kruger SE, Rebello JMA, Charlier J. Broadband ultrasonic backscattering applied to nondestructive characterization of materials. IEEE Trans Ultrason Ferroelect Freq Contr 2004;51:832–8.

[33] Pilchak AL, Li J, Rokhlin SI. Quantitative comparison of microtexture in near-alpha titanium measured by ultrasonic scattering and electron backscatter diffraction. Metall Mat Trans A 2014;45:4679–97.
[34] Ma C, Zhang Z, Luce B, Pusateri S, Xie B, Rafiei MH, Hu N. Accelerated design and characterization of non-uniform cellular materials via a machine-learning based framework. NPJ Comput Mater 2020;6:1–8.
[35] Jiang X, Jia B, Zhang G, Zhang C, Wang X, Zhang R, Yin H, Qu X, Song Y, Su L, Mi Z, Hu L, Ma H. A strategy combining machine learning and multiscale calculation to predict tensile strength for pearlitic steel wires with industrial data. Scr Mater 2020;186:272–7.
[36] Chen D, Xiao H, Xu J. An improved Richardson-Lucy iterative algorithm for C-scan image restoration and inclusion size measurement. Ultrasonics 2019;91:103–13.
[37] Iquebal AS, Pandagare S, Bukkapatnam S. Learning acoustic emission signatures from a nanoindentation-based lithography process: towards rapid microstructure characterization. Tribol Int 2020;143:106074.
[38] Jackson M, Dashwood R, Flower H, Christodoulou L. The microstructural evolution of near beta alloy Ti-10V-2Fe-3Al during subtransus forging. Metall and Mat Trans A 2005;36:1317–27.
[39] Wu C-H, Ho J-M, Lee DT. Travel-time prediction with support vector regression. IEEE Trans Intell Transport Syst 2004;5:276–81.
[40] Balogun O, Huber R, Chinn D, Spicer JB. Laser ultrasonic inspection of the microstructural state of thin metal foils. J Acoust Soc Am 2009;125:1437–43.
[41] Yang L, Lobkis OI, Rokhlin SI. Shape effect of elongated grains on ultrasonic attenuation in polycrystalline materials. Ultrasonics 2011;51:697–708.